Detailed modeling of combustion noise using a hydrodynamic/acoustic splitting model

By A. Giauque AND H. Pitsch

1. Motivation and objectives

Noise emissions from aircraft engines is an important problem, especially in the vicinity of airports. With innovative technologies such as double flux engines, jet noise has been drastically reduced during the past 20 years. Yet, with increasingly restrictive noise regulations, it is believed that further improvements will be obtained only through the reduction of combustion noise. Although direct combustion noise created by the interaction of heat release and pressure fluctuations has been known for more than a century (Rayleigh 1878), indirect combustion noise is now thought to be responsible for a major part of the overall noise emitted in the combustion chamber. Indirect combustion noise is due to entropy waves, which are created by the flame and accelerated by the flow, and thereby converted into acoustic waves. Experimental evidence of this phenomenon has been recently reviewed by Bake *et al.* (2007). However, the simulation of indirect noise and more generally speaking, of the overall acoustics is still a challenge in wall-bounded flows, where no acoustic far-field analogy can be used (Benoit & Nicoud 2005; Richter *et al.* 2005; Sattelmayer & Polifke 2005). In this work, instead of solving for the compressible reactive Navier-Stokes equations, a hydrodynamic/acoustic splitting approach is followed as suggested by Hardin & Pope (1994) and Goldstein (2003). The method derived by Seo & Moon (2006) for non-reactive cases is taken as a starting point and extended to reactive flows.

The main objective of the present paper is to develop a new technique for combustion noise studies by extending the Linear Compressible Perturbed Equations to reactive cases. The ability of this hybrid approach to represent the indirect combustion noise is assessed. The non-reactive implementation is tested for two co-rotating vortices in an unbounded domain, and is also validated in the case of a backward-facing step where interactions between walls and acoustic waves occur. Finally, a validation of the reactive implementation is provided for the case of a pulsating heat source dipole.

2. Theoretical background

2.1. *Extension of linear perturbed compressible equations to reactive cases*

The goal of the following derivation is to obtain transport equations for density, velocity and pressure fluctuations using the low-Mach number approximation of the flow as base solution. The compressible reactive Navier Stokes equations is:

$$\frac{\partial \rho}{\partial t} + \boldsymbol{\nabla}.\left(\rho \mathbf{v}\right) = 0, \tag{2.1}$$

$$\frac{\partial}{\partial t}\rho v_j + \boldsymbol{\nabla}.\left(\rho \mathbf{v} v_j\right) + \frac{\partial p}{\partial x_j} = \boldsymbol{\nabla}.\boldsymbol{\tau}_j, \tag{2.2}$$

$$\frac{\partial}{\partial t}\rho e_s + \boldsymbol{\nabla}.\left(\rho \mathbf{v} e_s\right) = -p\boldsymbol{\nabla}.\mathbf{v} - \boldsymbol{\nabla}.\mathbf{q} + \phi + \dot{\omega}_T, \tag{2.3}$$

where e_s is the sensible energy and ϕ is the dissipation function defined as $\phi = \tau_{ij}\partial v_i/\partial x_j$. The low-Mach number approximation of the Navier-Stokes equations are:

$$\frac{\partial \rho_0}{\partial t} + \boldsymbol{\nabla}.(\rho_0 \mathbf{v}_0) = 0, \tag{2.4}$$

$$\frac{\partial}{\partial t}\rho_0 v_{j0} + \boldsymbol{\nabla}.(\rho_0 \mathbf{v}_0 v_{j0}) + \frac{\partial p_2}{\partial x_j} = \boldsymbol{\nabla}.\boldsymbol{\tau}_{j0}, \tag{2.5}$$

$$\frac{\partial}{\partial t}\rho_0 e_{s0} + \boldsymbol{\nabla}.(\rho_0 \mathbf{v}_0 e_{s0}) = -p_0 \boldsymbol{\nabla}.\mathbf{v}_0 - \boldsymbol{\nabla}.\mathbf{q_0} + \dot{\omega}_{T0}, \tag{2.6}$$

where all variables have been decomposed using an asymptotic expansion in the Mach number (e.g., $v = v_0 + O(M^3)$). The asymptotic expansion of the pressure field is $p = p_0 + M^2 p_2 + O(M^3)$.

Subtracting Eqs. (2.4–2.6) from Eqs. (2.1–2.3), yields the following set of equations for pressure, velocity and density fluctuations with the low-Mach number approximation of the flow as baseflow:

$$\frac{\partial \rho'}{\partial t} + \boldsymbol{\nabla}.(\rho' \mathbf{v}) + \boldsymbol{\nabla}.(\rho_0 \mathbf{v}') = 0, \tag{2.7}$$

$$\frac{\partial}{\partial t}\left(\rho' v_j + \rho_0 v_j'\right) + \boldsymbol{\nabla}.\left(\rho' \mathbf{v} v_j + \rho_0 \mathbf{v}' v_j + \rho_0 \mathbf{v}_0 v_j'\right) = -\frac{\partial p'}{\partial x_j} + \boldsymbol{\nabla}.\boldsymbol{\tau'}_j, \tag{2.8}$$

$$\begin{aligned}\frac{\partial \alpha_0^\star p'}{\partial t} + p' \boldsymbol{\nabla}.\mathbf{v} + \boldsymbol{\nabla}.(\mathbf{v_0}\alpha_0^\star p') + \boldsymbol{\nabla}.(\mathbf{v}'\alpha^\star p) + p_0 \boldsymbol{\nabla}.\mathbf{v}' \\ = -\boldsymbol{\nabla}.\mathbf{q}' + \phi + \dot{\omega}_T' - p_2 \boldsymbol{\nabla}.\mathbf{v} - \boldsymbol{\nabla}.(\mathbf{v_0}\alpha_0^\star p_2) - \frac{\partial \alpha_0^\star p_2}{\partial t} - \frac{\partial \alpha^{\star'} p}{\partial t} - \boldsymbol{\nabla}.\left(\mathbf{v_0}\alpha^{\star'} p\right),\end{aligned} \tag{2.9}$$

where all fluctuations are defined as $f' = f - f_0$ except for the pressure fluctuation, which is defined as $p' = p - p_0 - p_2$. Finally, $\alpha^\star$ is defined as $\rho e_s/p$ and $\alpha_0^\star$ is equal to $\rho_0 e_{s0}/p_0$. It should be noted that Eqs. (2.7–2.9) have been obtained without taking any assumptions. They represent the non-linear evolution of the perturbed quantities defined as the subtraction of the baseflow to the complete flowfield. As such, when considering any variable obtained by the splitting method, the sum of its baseflow and perturbed components should match the same variable obtained by Direct Numerical Simulation as long as all the turbulent scales are resolved. Yet, because the two sets of equations (Eqs. (2.7–2.9) and Eqs. (2.4–2.6)) can be discretized differently both in space and time, the conservative properties of the entire system can be difficult to ensure numerically. Furthermore, the objective of the hydrodynamic/acoustic splitting methodology is to provide transport equations for the perturbations that will be solved on a different (usually coarser) mesh than the one used for the baseflow computation. This introduces an additional interpolation error in the full set of discretized equations that also influences mass, momentum and energy conservation. For these reasons, Seo & Moon (2006) report unphysical growth of vorticity modes in their simulations using this splitting methodology for nonreactive flows. Two main methods have been proposed to bound or remove vorticity fluctuations from the solution of Eqs. (2.7–2.9) or from their linear equivalent. The first method proposed by many authors (Bailly & Juve 2000; Seo & Moon 2006) is to modify the propagation operator itself. The second method proposed by Prax *et al.* (2008) consists of modifying only the source term of those equations so that it does not excite any vorticity modes.

In this work, the first approach is chosen because it can be properly justified by an

order of magnitude analysis in the low-Mach number limit (as proposed by Seo & Moon (2006)). Equations (2.7–2.9) can therefore be simplified in such a way that most source terms of fluctuating vorticity are neglected without degrading the quality of the acoustic predictions. Equations (2.7–2.9) are first linearized assuming that all fluctuations are small compared to their counterpart in the low-Mach number approximation.

$$\frac{D\rho'}{Dt} + \boldsymbol{\nabla}.(\rho_0 \mathbf{v}') = 0, \tag{2.10}$$

$$\frac{D_0 v_j'}{Dt} + \mathbf{v}'.\boldsymbol{\nabla}(v_{j0}) + \frac{1}{\rho_0}\frac{\partial p'}{\partial x_j} + \frac{\rho'}{\rho_0}\frac{D_0 v_{j0}}{Dt} = \frac{1}{\rho_0}\boldsymbol{\nabla}.\boldsymbol{\tau'}_j, \tag{2.11}$$

$$\begin{aligned}\frac{D_0 p'}{Dt} + \frac{p'}{\alpha_0^\star}\frac{D\alpha_0^\star}{Dt} + \frac{p'\boldsymbol{\nabla}.\mathbf{v}_0}{\alpha_0^\star} + \frac{\boldsymbol{\nabla}.(\alpha_0^\star(p_0+p_2)\mathbf{v}')}{\alpha_0^\star} + \frac{(p_0+p_2)\boldsymbol{\nabla}.\mathbf{v}'}{\alpha_0^\star} = \\ + \frac{-\boldsymbol{\nabla}.\mathbf{q}' + \phi + \dot{\omega}_T'}{\alpha_0^\star} - \frac{p_2\boldsymbol{\nabla}.\mathbf{v}_0}{\alpha_0^\star} - \frac{1}{\alpha_0^\star}\frac{D\alpha_0^\star p_2}{Dt} - \frac{1}{\alpha_0^\star}\frac{D\alpha^{\star'}(p_0+p_2)}{Dt},\end{aligned} \tag{2.12}$$

where $D_0 f/Dt = \partial f/\partial t + \mathbf{v_0}.\boldsymbol{\nabla}(f)$ and $Df/Dt = \partial f/\partial t + \boldsymbol{\nabla}.(\mathbf{v}_0 f)$.
Using the vector identity $\mathbf{v_0}.\boldsymbol{\nabla}(\mathbf{v}') + \mathbf{v}'.\boldsymbol{\nabla}(\mathbf{v}_0) = \boldsymbol{\nabla}(\mathbf{v}'.\mathbf{v}_0) + \boldsymbol{\omega'}\times\mathbf{v}_0 + \boldsymbol{\Omega}\times\mathbf{v}'$, Eq. (2.11) is rewritten as:

$$\frac{\partial \mathbf{v}'}{\partial t} + \boldsymbol{\nabla}(\mathbf{v}'.\mathbf{v}_0) + \boldsymbol{\omega'}\times\mathbf{v}_0 + \boldsymbol{\Omega}\times\mathbf{v}' + \frac{1}{\rho_0}\boldsymbol{\nabla}p' + \frac{\rho'}{\rho_0}\frac{D_0\mathbf{v}_0}{Dt} = \frac{1}{\rho_0}\boldsymbol{\nabla}.\boldsymbol{\tau'}, \tag{2.13}$$

where $\boldsymbol{\omega'} = \boldsymbol{\nabla}\times\mathbf{v}'$ and $\boldsymbol{\Omega} = \boldsymbol{\nabla}\times\mathbf{v}_0$.

To further simplify the formulation, a wave equation for pressure fluctuations is derived and the Mach number dependence of each term is examined. The low-Mach number variables are scaled by their freestream values: $\rho_0 \approx \rho_\infty$, $\mathbf{v}_0 \approx \mathbf{v}_\infty$, $p_2 \approx \rho_\infty \mathbf{v}_\infty^2$, $p_0 \approx \rho_\infty c_\infty^2$. The perturbed variables are scaled using the perturbed velocity scaling $\mathbf{v}' \approx M\mathbf{v}_\infty$ and the linear acoustics scalings $p' \approx \rho_\infty c_\infty \mathbf{v}'$ and $\rho' \approx (\rho_\infty/c_\infty)\mathbf{v}'$. Time is scaled by l/c_∞, where l is the reference length and c_∞ is the reference speed of sound.
Multiplying the divergence of Eq. (2.13) by $(\alpha_0^\star+1)/\alpha_0^\star.(p_0+p_2)$ and subtracting the result from the time derivative of Eq. (2.12) leads to

$$\begin{aligned}&\underbrace{\frac{\partial^2 p'}{\partial t^2}}_{O(M^1)} + \underbrace{\frac{\partial}{\partial t}\frac{p'}{\alpha_0^\star}\boldsymbol{\nabla}.\mathbf{v}_0}_{O(M^2)} + \underbrace{\frac{\partial \mathbf{v}_0.\boldsymbol{\nabla}p'}{\partial t}}_{O(M^2)} - \underbrace{\gamma_0^\star(p_0+p_2)\boldsymbol{\nabla}.\left(\frac{1}{\rho_0}\boldsymbol{\nabla}p'\right)}_{O(M^1)} + \underbrace{\frac{\partial}{\partial t}\gamma_0^\star(p_0+p_2)\boldsymbol{\nabla}.(\mathbf{v}')}_{O(M^1)} \\ &+ \underbrace{\frac{\partial}{\partial t}\left(\frac{\mathbf{v}'}{\alpha_0^\star}.\boldsymbol{\nabla}\alpha_0^\star(p_0+p_2)\right)}_{O(M^1)} + \underbrace{\frac{\partial}{\partial t}\left(\frac{p'}{\alpha_0^\star}\frac{D\alpha_0^\star}{Dt}\right)}_{O(M^1)} = \underbrace{-\frac{\partial}{\partial t}\frac{p_2}{\alpha_0^\star}\boldsymbol{\nabla}.\mathbf{v}_0}_{O(M^2)} - \underbrace{\frac{\partial}{\partial t}\left(\frac{1}{\alpha_0^\star}\frac{D\alpha_0^\star p_2}{Dt}\right)}_{O(M^1)} \\ &+ \underbrace{\gamma_0^\star(p_0+p_2)\boldsymbol{\nabla}.\left(\boldsymbol{\Omega_0}\times\mathbf{v}' + \boldsymbol{\omega}'\times\mathbf{v}_0 + \frac{\rho'}{\rho_0}\frac{D_0\mathbf{v}_0}{Dt} + \boldsymbol{\nabla}(\mathbf{v}'.\mathbf{v}_0) - \frac{1}{\rho_0}\boldsymbol{\nabla}.\boldsymbol{\tau'}\right)}_{O(M^2)} \\ &+ \underbrace{\frac{\partial}{\partial t}\frac{1}{\alpha_0^\star}\left(-\frac{\partial q_i'}{\partial x_i}\right)}_{O(M^2)} + \underbrace{\frac{\partial}{\partial t}\frac{\phi}{\alpha_0^\star}}_{O(M^2)} + \underbrace{\frac{\partial}{\partial t}\frac{\dot{\omega}_T'}{\alpha_0^\star}}_{O(M^1)} - \underbrace{\frac{\partial}{\partial t}\left(\frac{1}{\alpha_0^\star}\frac{D\alpha^{\star'}(p_0+p_2)}{Dt}\right)}_{O(M^1)},\end{aligned} \tag{2.14}$$

where $\gamma_0^\star = (\alpha_0^\star+1)/\alpha_0^\star$.

Each term has order of $\rho_\infty c_\infty^3 U_\infty/l^2$ multiplied by a Mach number to the power denoted in Eq. (2.14). Identifying $O(M^2)$ terms in Eq. (2.14) and neglecting the corresponding terms in Eq. (2.13) responsible for vorticity production, leads to the Reactive Linear

Perturbed Compressible Equations (RLPCE):

$$\frac{D\rho'}{Dt} + \boldsymbol{\nabla}.(\rho_0 \mathbf{v}') = 0, \tag{2.15}$$

$$\frac{\partial v_j'}{\partial t} + \boldsymbol{\nabla}(\mathbf{v}'.\mathbf{v}_0) + \frac{1}{\rho_0}\frac{\partial p'}{\partial x_j} = 0, \tag{2.16}$$

$$\frac{D_0 p'}{Dt} + \frac{p'}{\alpha_0^\star}\frac{D\alpha_0^\star}{Dt} + \gamma_0^\star(p_0+p_2)\boldsymbol{\nabla}.\mathbf{v}' + \frac{\mathbf{v}'.\boldsymbol{\nabla}\left(\alpha_0^\star(p_0+p_2)\right)}{\alpha_0^\star} = -\frac{1}{\alpha_0^\star}\frac{D\alpha_0^\star p_2}{Dt} - \frac{1}{\alpha_0^\star}\frac{D\alpha^{\star'}(p_0+p_2)}{Dt} + \frac{\dot{\omega}_T'}{\alpha_0^\star}. \tag{2.17}$$

A generalized acoustic analogy has been developed by Goldstein (2003) for non-reactive and homogeneous flows. It can be shown that by setting $\alpha^\star = 1/(\gamma-1) =$ constant and $\dot{\omega}_T' = 0$, Eqs. (2.15–2.17) reduce to the linearization of the equations describing this acoustic analogy.

One can now compare the linear transport equation for the perturbed vorticity (Eq. (2.18)) obtained by taking the curl of Eq. (2.13) to the Eq. (2.19) that can be formed by taking the curl of Eq. (2.16).

$$\frac{\partial \boldsymbol{\omega'}}{\partial t} = -\boldsymbol{\nabla}\times(\boldsymbol{\omega'}\times\mathbf{v}_0 + \boldsymbol{\Omega}\times\mathbf{v}') - \boldsymbol{\nabla}\times\frac{\rho'}{\rho_0}\frac{D_0\mathbf{v}_0}{Dt} + \boldsymbol{\nabla}\times\frac{1}{\rho_0}\boldsymbol{\nabla}.\boldsymbol{\tau'} - \boldsymbol{\nabla}\times\left(\frac{1}{\rho_0}\boldsymbol{\nabla}p'\right) \tag{2.18}$$

$$\frac{\partial \boldsymbol{\omega'}}{\partial t} = -\boldsymbol{\nabla}\times\left(\frac{1}{\rho_0}\boldsymbol{\nabla}p'\right). \tag{2.19}$$

Most of the fluctuating vorticity production terms have been neglected as they scale with second or higher order in the Mach number decomposition. Yet, one can notice that because of the spatially varying baseflow density field, the source is not identically zero as for the case of non-reactive flows. This point will be addressed in subsequent studies.

2.2. *Entropy noise and acoustic source*

The main goal of this study is to provide a hydrodynamic/acoustic splitting methodology able to compute the indirect noise in aircraft engines. Because the low-Mach number approximations of the flow variables are now used to provide the acoustic sources, some physical phenomena have been neglected. One therefore has to first ensure that the interaction between the entropy modes created by the flame and the flow is retained in the baseflow.

By using Gibbs' relation between entropy, temperature and density fluctuations and differentiating the equation of state, assuming that the thermodynamic pressure is constant, one can relate the fluctuation of entropy to the fluctuation of density in the flow:

$$\frac{s"}{C_p} = -\frac{\rho"}{\rho_0}. \tag{2.20}$$

Note that $f"$ represents the fluctuation of the low-Mach number baseflow variable f due to the introduction of the entropy wave. Equation (2.20) shows that introducing an entropy fluctuation in the baseflow is therefore identical to introducing the proper density fluctuation in the flow. Assuming that all fluctuations $\bullet"$ are small compared to the initial low-Mach number approximation of the flow $\bullet_0$, one can write the perturbed

equations for momentum and density:

$$\frac{\partial \rho"}{\partial t} + \frac{\partial \rho" v_0}{\partial x} + \frac{\partial \rho_0 v"}{\partial x} = 0 \tag{2.21}$$

$$-v_0 \frac{\partial \rho"}{\partial t} + \frac{\partial \rho_0 v"}{\partial t} + 2\rho_0 v" \frac{\partial v_0}{\partial x} + \frac{\partial p"}{\partial x} = 0. \tag{2.22}$$

Combining both equations leads to the following expression for the perturbation of the pressure gradient:

$$\frac{\partial p"}{\partial x} = v_0 \frac{\partial \rho"}{\partial t} + \frac{\partial}{\partial t} A_x \left(\frac{\partial \rho"}{\partial t} + \frac{\partial \rho" v_0}{\partial x} \right) + 2A_x \left(\frac{\partial \rho"}{\partial t} + \frac{\partial \rho" v_0}{\partial x} \right) \frac{\partial v_0}{\partial x}, \tag{2.23}$$

where $A_x(f)$ is the indefinite integral of function f.
As the time derivative operator commutes with A_x, we find:

$$\frac{\partial p"}{\partial x} = v_0 \frac{\partial \rho"}{\partial t} + A_x \left(\frac{\partial^2 \rho"}{\partial t^2} + \frac{\partial}{\partial x} v_0 \frac{\partial \rho"}{\partial t} \right) + 2A_x \left(\frac{\partial \rho"}{\partial t} + \frac{\partial \rho" v_0}{\partial x} \right) \frac{\partial v_0}{\partial x}. \tag{2.24}$$

If one assumes that during the acoustic time scale, the time derivative of the density fluctuation is negligible (which means that the entropy source remains steady as noise is created), the perturbation of the low-Mach number approximation of the pressure gradient simplifies to:

$$\frac{\partial p"}{\partial x} = 2\rho" v_0 \frac{\partial v_0}{\partial x}, \tag{2.25}$$

which, using the identity between entropy and density fluctuations, can be rewritten as:

$$\frac{\partial p"}{\partial x} = -2\rho_0 v_0 \frac{\partial v_0}{\partial x} \frac{s"}{C_p}. \tag{2.26}$$

If Eq.(2.26) is then substituted into Eq.(2.17), its source term is:

$$S = 2A_x(\rho_0 v_0 \frac{\partial v_0}{\partial x} \frac{s"}{C_p}) \frac{\partial}{\partial x} v_0 + 2\rho_0 v_0^2 \frac{\partial v_0}{\partial x} \frac{s"}{C_p}. \tag{2.27}$$

The last term is formally identical to the one present in the analysis of Marble & Candel (1977). This means that the present approach is able to represent the interaction between incoming entropy waves and the low-Mach number baseflow. As demonstrated in Marble & Candel (1977), this interaction is the cause of sound created when high-temperature spots interact with large gradients of velocity. This is believed to be the reason for the so-called "indirect combustion noise" observed experimentally in turbo engines (Bake *et al.* 2007).

3. Results

3.1. *Numerical method*

A solver for the set of Eqs. (2.15-2.17) as been developed. For this, the framework of NGA code has been used. NGA is a structured, finite-difference code that is staggered in time and space. This code has been developed for accurate DNS and LES computations (Desjardin *et al.* 2008). The RLPC equations are solved explicitly in order to avoid communications between processors, which are needed for an implicit solution of the equations. This choice is also motivated by the fact that the acoustic CFL number should not be greater than 1, which makes an implicit solver less attractive. The time advancement is made through an optimized sixth-order Runge-Kutta algorithm developed

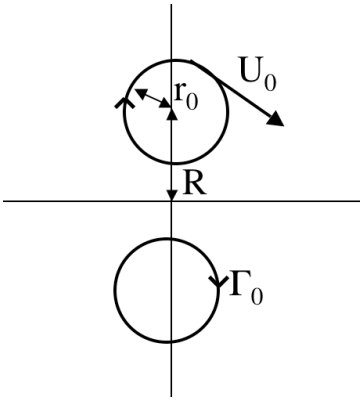

FIGURE 1. Schematic flow configuration of the pair of co-rotating vortices.

by Bogey & Bailly (2004). In this study, sixth-order finite-difference spatial operators are used. This implementation requires to remove the time staggering of the NGA code. Yet, the advantages of spatial staggering compared to a collocated scheme are kept. This has the advantage that, compared with a collocated formulation, for a given order of accuracy and a specified number of grid-points, a better transport of acoustic waves is expected.

3.2. *Pair of rotating vortices*

In order to test the accuracy of the solver, a simple unconfined test case is first presented. The sound emitted by two co-rotating vortices is computed. Figure 1 shows the general setup of the numerical experiment. In this case, the rotation Mach number (M_r) based on the maximum rotation velocity is equal to 0.3 in order to test the solver at the limit of validity of the low-Mach number approximation. Other parameters are the half distance between the centers of the two vortices $R = 0.0036$ m, the speed of sound $c_0 = 340.81$ m/s, and $r_0 = 7.92 \times 10^{-4}$ m, which is the distance from the center of each vortex at which the velocity is maximum. The domain size of the simulation is 1.4 m $\times$ 1.4 m. The period of rotation of the two vortices around each other is $T = 8\pi^2 R^2/\Gamma_0$. The system formed by the two vortices behaves like an acoustic quadrupole with a frequency equal to $T_a = 2T$. In our case $T = 1988$ Hz. The analytic solution for the acoustic pressure evolution in the limit case of point vortices has been derived by Moehring (1978). Using DNS, Mitchell *et al.* (1999) have shown the analytical solution to be accurate in the case of finite viscous vortices. Equation (3.1) provides an analytical relation between the physical quantities describing the flow and the emitted sound:

$$p'(r,\theta,t) = -\frac{\rho_0 \Gamma_0^4}{64\pi^3 R^4 c_0^2}\left(J_2\left(\frac{2\Omega_0 r}{c_0}\right) sin(2\theta + 2\Omega_0 t) + Y_2\left(\frac{2\Omega_0 r}{c_0}\right) cos(2\theta + 2\Omega_0 t)\right), \tag{3.1}$$

where J_2 and Y_2 are the Bessel's functions of the first and second kind, respectively. Figure 2 shows a snapshot of the instantaneous acoustic pressure. The characteristic spiral pattern is well-captured by the solver. Figure 3 shows a quantitative comparison of the temporal signal of acoustic pressure obtained on the horizontal axis at a distance equal to two wavelengths with the analytical solution provided by Eq. (3.1). The result is in good agreement with the analytical expression except for a slight difference in the

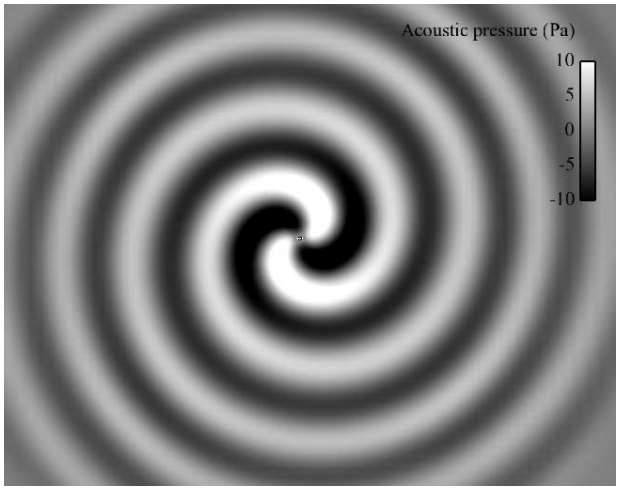

FIGURE 2. Snapshot of the acoustic pressure field. Note the double spiral pattern and the nearly cylindrical nature of the waves in the far field.

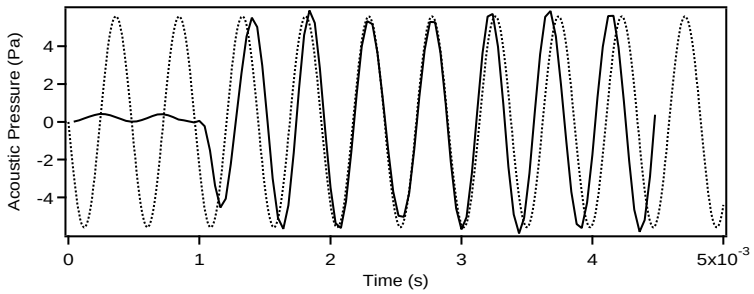

FIGURE 3. Far-field pressure traces at $r/\lambda = 2$ showing the results of the simulation (——), and the prediction of Eq. (3.1) (·····). Both measurement points are located on the positive horizontal axis.

frequency of the phenomenon, which could be related to the error in the computation of the low-Mach number sources at Ma= 0.3.

3.3. *Backward-facing step*

In order to verify the accuracy and stability of the formulation when both open boundaries and reflecting walls are present, the case of a backward-facing step is computed for different far-field Mach numbers. The noise emitted by such flows is of interest in many applications and the backward-facing step case has therefore been extensively studied in the past, both experimentally (Armaly *et al.* 1983) and numerically (Le *et al.* 1997). The directivity of the sound pressure level (SPL) as well as the evolution of its amplitude with the Mach number have been measured by Jacob *et al.* (2001).

A schematic representation of the 2-D mesh used in this study is shown in Fig. 4. Figure 5(a) shows a snapshot of the fluctuating pressure field at Ma= 0.1 and Fig. 5(b) shows the recirculation vortex induced by the flow at the same instant. One observes that the origin of the acoustic waves is close to the center of the recirculation vortex.

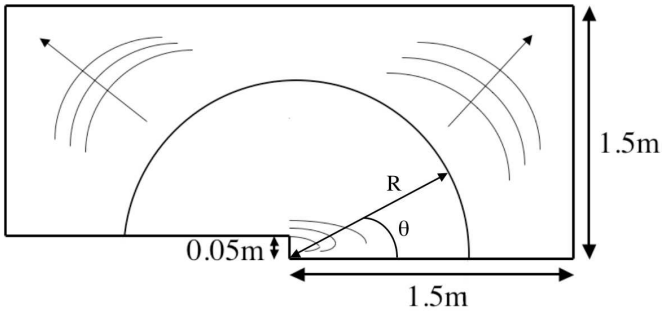

FIGURE 4. Schematic flow configuration of the backward facing step.

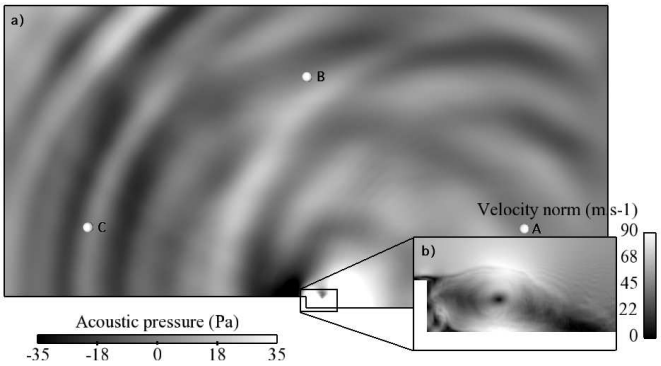

FIGURE 5. Snapshot of flow variables: a) acoustic pressure b) velocity norm. Notice the strong backward pressure wave emission. White markers (A,B,C) show the locations of SPL measurements.

One also observes the characteristic backscattering of acoustic waves typical of this type of flow.

Figure 6 presents the directivity pattern of the SPL at Ma= 0.1, 0.15 and 0.2. The SPL directivity shows a strong dipole contribution as observed experimentally by Howe (1997). The SPL directivity flattens out as the Mach number increases, showing only a small back and front preference at Ma= 0.2. Although, because of the confinement of acoustic waves in 2-D the absolute amplitude of the SPL cannot be directly compared to experiments, the evolution of the SPL amplitude with increasing Mach number can be compared to fitting functions derived from experimental measurements (Jacob *et al.* 2001). Figure 7 shows this comparison at the points A, B and C indicated in Fig. 5 located on the 1 m radius circle shown in Fig. 4. The corresponding angles to the three points are respectively 30°, 90° and 150°. The agreement with experimental results is good except at point B (90°) where the growth rate of the SPL as a function of the Mach number is slightly over-estimated. The capability of the 2-D simulation to show the correct trends can be explained by the fact that the vortex located behind the step is responsible for the major part of the emitted noise (Armaly *et al.* 1983; Le *et al.* 1997). Therefore, although a 3-D simulation would be required to capture the additional influence of a realistic turbulence, this 2-D simulation is sufficient to accurately obtain the main fluctuations of the Lamb vector ($\mathbf{L}=(\boldsymbol{\omega}\times\mathbf{u})'$ where $\boldsymbol{\omega}$ is the vorticity) at the

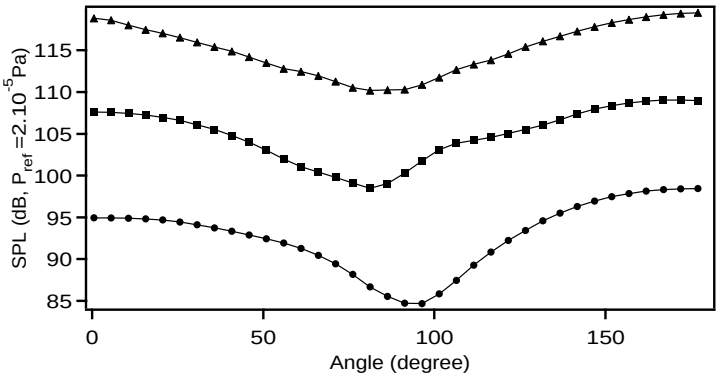

FIGURE 6. Computed SPL along a 1 m radius circle centered on the step for different far-field Mach numbers. Ma= 0.1 : •, Ma= 0.15 : ■, Ma= 0.2 : ▲.

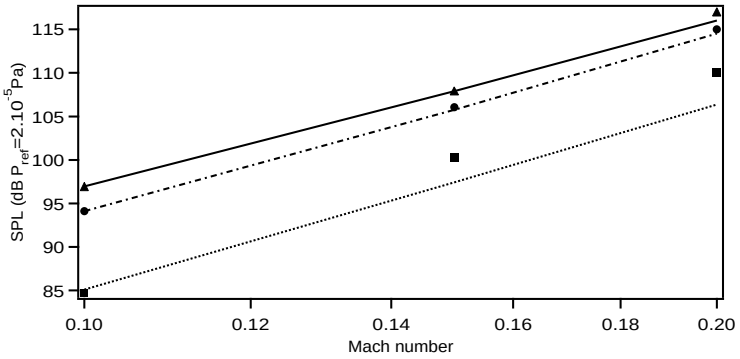

FIGURE 7. SPL versus Mach number. Computed data at 30° (Point A): •, 90° (Point B): ■, and 150° (Point C): ▲. Experimental fit at 30° : -·-·- , 90° : ····· , and 150° : —— (Jacob *et al.* 2001).

origin of the noise. This shows that both the strength of the acoustic sources as well as the propagation of the acoustic waves are accurately computed by the solver. It also demonstrates that the reflection of acoustic waves by the walls is correctly handled by the solver.

3.4. *Fluctuating temperature dipole*

In order to test the accuracy of the hydrodynamic/acoustic splitting method in the presence of temperature and density fluctuations, the noise emitted by a fluctuating temperature dipole is computed. Two Gaussian-shaped fluctuating temperature spots are oscillating with opposite phases at a distance $2a$ from each other.

In this case, pressure fluctuations are given by a cylindrical wave equation assuming the baseflow velocity induced by the temperature change is negligible:

$$\frac{1}{c_0^2}\frac{\partial^2 p'}{\partial t^2} - \frac{1}{r}\frac{\partial}{\partial r}\left(r\frac{\partial p'}{\partial r}\right) = \frac{\partial S(r,\theta,t)}{\partial t}, \tag{3.2}$$

where $S(r,\theta,t)$ is the right-hand side of Eq. (2.17), which reduces in this case to $S(r,\theta,t) = -\partial p_2/\partial t$ by neglecting the effect of the temperature change on the thermodynamic

properties of the gas. On the other hand, this source term can also be decomposed as $S(r,\theta,t) = (f(r_+) - f(r_-))\sin(\omega \mathrm{t})$, ω is the pulsing frequency of the dipole. The functions $f(r+)$ and $f(r_-)$ are the two monopole contributions of the dipole located on the horizontal axis at a distance a and -a from the origin.

Equation (3.3) describes the analytical solution of the pressure fluctuation induced by an acoustic dipole in 2-D cylindrical coordinates using the free-field Green's function of the pressure wave operator:

$$p'(r,\theta,t) = f(r_+) * \partial G(r_+,t)/\partial t + f(r_-) * \partial G(r_-,t)/\partial t. \tag{3.3}$$

In cylindrical coordinates, $G(r,t) = i/(4c_0^2)H^1_{(0)}(\omega r/c_0)$, where $H^1_{(0)}$ is the Hankel function of the first kind.

The source strength $f(r)$ can be determined for each monopole contribution using the perturbed low-Mach equations (Eqs. (2.21–2.22)) and the linearized low-Mach number perturbed state equation (Eq. (3.4)).

$$\frac{p"}{p_0} = \frac{\rho"}{\rho_0} + \frac{T"}{T_0}. \tag{3.4}$$

In cylindrical coordinates, the following relation between pressure and temperature fluctuations is obtained:

$$p"(r,\theta,t) = \frac{\rho_0}{T_0}\frac{\partial^2 A_r(A_r(T"))}{\partial t^2}, \tag{3.5}$$

where A_r is the indefinite integral with respect to the radial coordinate.
The temperature forcing imposed at each time step is described by

$$T"(r,\theta,t) = \Delta_T \left(e^{-r_+^2} - e^{-r_-^2}\right)\sin(\omega \mathrm{t}), \tag{3.6}$$

where $r_+ = \sqrt{(x-a)^2+y^2}/(\sqrt{2}\sigma)$, and $r_+ = \sqrt{(x+a)^2+y^2}/(\sqrt{2}\sigma)$. In our case, $\sigma = 2$ mm.
This forcing is therefore creating a low-Mach number perturbed pressure given by:

$$p"(r',t) = \frac{2\sigma^2\omega^2\rho_0\Delta_T}{T_0}\left(r'(\mathrm{erf(r')} - 1) + \frac{1}{\sqrt{\pi}}\mathrm{e}^{-\mathrm{r}'^2}\right)\sin(\omega \mathrm{t}), \tag{3.7}$$

where erf is the error function defined as $\mathrm{erf(x)} = \int_{-\infty}^{\mathrm{x}} \mathrm{e}^{-\mathrm{x}'^2}\mathrm{dx}'$. Using the linearity of the perturbed low-Mach number equations (Eqs. (2.21–2.22)), the analytical baseflow perturbed pressure field therefore becomes:

$$\begin{aligned} p"(r,\theta,t) = {} & \underbrace{\frac{2\sigma^2\omega^2\rho_0\Delta_T}{T_0}}_{P_0}\underbrace{\left(r_+(\mathrm{erf(r_+)} - 1) + \frac{1}{\sqrt{\pi}}\mathrm{e}^{-\mathrm{r}_+^2}\right)}_{\Theta_+} sin(\omega t) \\ & - \frac{2\sigma^2\omega^2\rho_0\Delta_T}{T_0}\underbrace{\left(r_-(\mathrm{erf(r_-)} - 1) + \frac{1}{\sqrt{\pi}}\mathrm{e}^{-\mathrm{r}_-^2}\right)}_{\Theta_-}\sin(\omega t). \end{aligned} \tag{3.8}$$

Substituting Eq. (3.8) into Eq. (3.3), yields the sound generated by the fluctuating temperature dipole:

$$p'(r,\theta,t) = \frac{\omega^2}{4c_0^2}P_0\left[\Theta_+ * H^1_{(0)}\left(\frac{\sqrt{2}\sigma\omega}{c_0}r_+\right) - \Theta_- * H^1_{(0)}\left(\frac{\sqrt{2}\sigma\omega}{c_0}r_-\right)\right]. \tag{3.9}$$

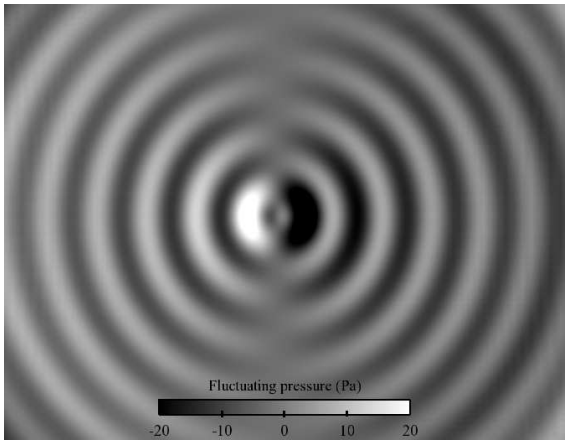

FIGURE 8. Snapshot of the acoustic pressure. Note the dipole structure of the emitted noise.

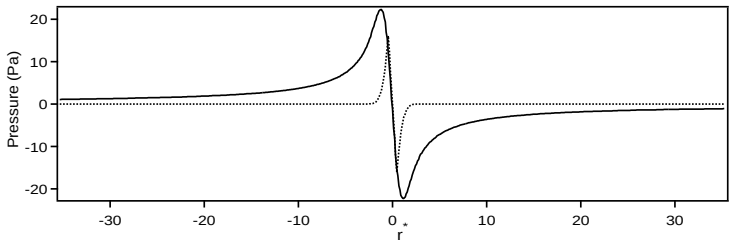

FIGURE 9. Low-Mach number pressure along the x-axis. Computation: ——— , analytical result (Eq.3.8): ····· . $r^* = r/\sqrt{2}\sigma$.

Figure 8 shows a snapshot of the acoustic pressure field which displays a characteristic dipole structure. The maximum amplitude of the signal is just above 20 Pa. Yet, the maximum amplitude predicted by Eq. (3.9) is much higher than this value. To understand this discrepancy, Fig. 9 compares the maximum amplitude of the computed baseflow pressure field with the one provided by Eq. (3.8). Figure 9 shows that the assumption of the baseflow velocity induced by the temperature change to be negligible is not valid in this case.

However, assuming a two-point source dipole, the spatial distribution of the sound waves is given by the following combination of Hankel's functions:

$$\left[H^1_{(0)}\left(\frac{\sqrt{2}\sigma\omega}{c_0} r_+\right) - H^1_{(0)}\left(\frac{\sqrt{2}\sigma\omega}{c_0} r_-\right)\right].$$

Figure 10 shows a comparison between the normalized pressures obtained, superposing the previous expression and the computation. It reveals that the wavelength of the acoustic pressure as well as the decrease of the amplitude with increasing radial coordinate are correctly predicted by the solver.

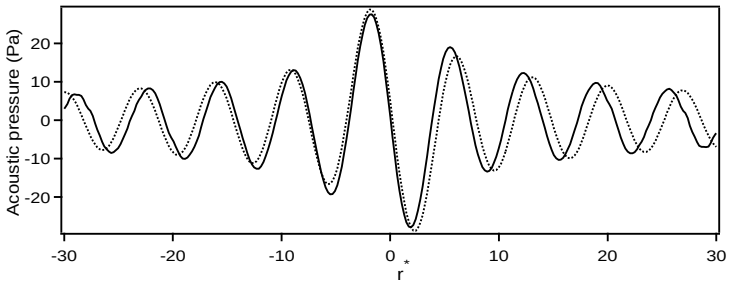

FIGURE 10. Normalized acoustic pressure at $t = 2.135e^{-3}s$. Computation: ——— , analytical result: ····· . $r^* = r/\sqrt{2}\sigma$.

4. Concluding remarks

A hydrodynamic/acoustic splitting method for acoustic computations in reactive flows has been proposed. First, a low-Mach approximation of the flow variables is computed which provides the source terms for a set of Reactive Perturbed Compressible Linear Equations (RPCLE). Solving RPCL equations provides the noise emitted by the flow. It is also shown that the indirect combustion noise production term is actually present in the sources of the RPCL equations. As expected in the non-reactive flows, these equations simplify to the original PCLE given by Seo & Moon (2006) and are consistent with the linearization of Goldstein's generalized acoustic analogy equations (Goldstein 2003). Results are shown to match analytical predictions and experimental trends in homogeneous flow test cases.

RPCL equations are intended to provide the noise emitted in combustion chambers. For this purpose a dipole case is computed, which corresponds to a fluctuating temperature and density field. It shows encouraging results when compared with analytical predictions. However, the direct noise emitted by a flame has a known monopole contribution to the SPL. Despite the good predictions of the dipole source, the monopole is not yet correctly represented by the method. This issue is related to the determination of the baseflow pressure in cases for which the total mass in the system is constantly changing with time. This problem will be investigated in further studies.

Acknowledgements

This work is supported by NASA. The authors thank Dr. Anne-Laure Birbaud, Christoph Schmitt, Dr. Fabrizio Bisetti, and Dr. Madhusudan Pai for many useful discussions and for their help during the preparation of this article.

REFERENCES

ARMALY B. F., DURST F., PEREIRA J. C. F. & SCHNUNG, B. 1983 Experimental and theoretical investigation of backward-facing step flow. *J. Fluid Mech.* **127**, 473–496.

BAILLY C. & JUVE D. 2000 Numerical simulation of acoustic propagation problems using linearized Euler equations. *AIAA Journal* **38** (1), 22–29.

BOGEY C. & BAILLY C. A family of low dispersive and low dissipative explicit schemes for flow and noise computations. *Journal of Computational Physics*, **194** (1), 194–214.

Bake F., Michel U. & Roehle I. 2007 Investigation of Entropy Noise in Aero-Engine Combustors. *Transactions of the ASME* **129** (2), 370–376.

Benoit L. & Nicoud F. 2005 Numerical assessment of thermo-acoustic instabilities in gas turbines. *International Journal for Numerical Methods in Fluids* **47** (8-9), 849–855.

Chu B. T. & Kovasznay L. S. G. 1958 Non-linear interactions in a viscous heat-conducting compressible gas. *J. Fluid Mech.* **3** (5), 494–514.

Desjardin O., Blanquart G., Balarac G. & Pitsch H. 2008 High order conservative finite difference scheme for variable density low Mach number turbulent flows. *Journal of Computational Physics* **227** (15), 7125–7159.

Goldstein. M. E. 2003 A generalized acoustic analogy. *J. Fluid Mech.* **488**, 315–333.

Hardin J. C.. & Pope D. S. 1994 An acoustic/viscous splitting technique for computational aeroacoustics. *Theoretical Computational Fluid Dynamics* **6** (5-6), 323–340.

Howe M. S. 1997 Influence of separation on sound generated by vortex interaction. *AIAA Journal* **11** (8), 857–872.

Jacob M. C., Louisot A. & Juve D. 2001 Experimental study of sound generated by backward-facing steps under wall jet. *AIAA Journal* **39** (7), 1254–1260.

Le H., Moin P. & Kim J. 1997 Direct numerical simulation of turbulent flow over a backward-facing step. *J. Fluid Mech.* **330**, 349–374.

Marble F. E. & Candel S. M. 1977 Acoustic disturbance from gas non-uniformities convected through a nozzle. *Journal of Sound and Vibration* **55**, 225–243.

Mitchell B. E., Lele S. K. & Moin P. 1995 Direct computation of the sound from a compressible co-rotating vortex pair. *J. Fluid Mech.* **285**, 181–202.

Moehring B. E. 1978 On vortex sound at low Mach number. *J. Fluid Mech.* **85** (4), 685–691.

Prax C., Golanski F. & Nadal L. Control of the vorticity mode in the linearized Euler equations for hybrid aeroacoustic prediction. *Journal of Computational Physics* **227** (12), 6044–6057.

Rayleigh L. 1878 The explanation of certain acoustical phenomena. *Nature* **18**, 319–321.

Richter C., Panek L. & Thiele F. H. 2005 On the application of CAA-methods for the simulation of indirect combustion noise. 11th AIAA/CEAS Aeroacoustics Conference, Monterey, California. May 23–25 **AIAA-2919**.

Sattelmayer, T. & Polifke, W. 2005 Assessment of methods for the computation of the linear stability of combustors. *Combustion Science and Technology* **175** (3), 453–476.

Seo J. H. & Moon Y. J. 2006 Linearized perturbed compressible equations for low Mach number aeroacoustics. *Journal of Computational Physics* **218** (2), 702–719.